This full text paper was peer-reviewed at the direction of IEEE Instrumentation and Measurement Society prior to the acceptance and publication

MCNP-FBSM: Development of MCNP/MCNPX Source Model for Simulation of Multi-Slice Fan-Beam X-Ray CT Scanners

Hamidreza Khodajou-Chokami, *Member, IEEE*, Seyed Abolfazl Hosseini, Mohammad Reza Ay, *Member, IEEE*, Habib Zaidi, *Member, IEEE*

***Abstract*—Computed tomography (CT) is one of the most valuable diagnostic imaging tools in the clinic and is widely used worldwide. One of the main motivations driving research and development in CT is to achieve better image quality while keeping the radiation dose to the patient as low as possible. In this regard, computer simulations play a key role in the optimization of CT design. In this work, a fan-beam source model (FBSM) for the simulation of multi-slice fan-beam CT scanners using the MCNP Monte Carlo code, has been developed and implemented. The use of this model removes the need for using the collimator in the system configuration and thus to overcome the perennial problem of particle starvation imposed by the collimator. The accuracy of our developed MCNP-FBSM model was evaluated through comparison with previously published experimental results demonstrating good agreement. Therefore, the MCNP-FBSM based CT simulator is a powerful tool for protocol design, optimization of geometrical design parameters, assessment of image reconstruction algorithms and evaluating future innovations to improve the performance of CT scanners.**

***Keywords*—Computed Tomography imaging, Monte Carlo simulations, image reconstruction, MCNP-FBSM, modeling.**

I. Introduction

COMPUTED tomography (CT) is one of the valuable diagnostic tools in clinical imaging. The main motivation for the development of novel CT scanner designs is the further improvement in performance to enable diagnosis of the disease in its early stages. Moving from single-slice to multi-slice and single energy to dual-energy and the spectral imaging are the major advancements in CT technology.

This work was supported in part by Sharif University of Technology under a Graduate Research Program Grant.

H. Khodajou-Chokami is with the Group of Medical Radiation Engineering, Department of Energy Engineering, Sharif University of Technology, Tehran, Iran (e-mail: hamidreza.khodajou@gmail.com).

S. A. Hosseini is with the Group of Medical Radiation Engineering, Department of Energy Engineering, Sharif University of Technology, Tehran, Iran (e-mail: sahosseini@sharif.edu).

M. R. Ay is with the Department of Medical Physics and Biomedical Engineering, Tehran University of Medical Sciences, Tehran, Iran (e-mail: mohammadreza_ay@tums.ac.ir).

H. Zaidi is with the Department of Medical Physics and Biomedical Engineering, Tehran University of Medical Sciences, Tehran, Iran (habib.zaidi@hcuge.ch).

The bulk of CT research to date focuses on the design and improvement of overall system performance, development of image analysis techniques and improvement of image quality while reducing patient dose at the same time. These aims could be achieved through costly empirical measurements and/or the development and fabrication of prototypes [1-10], Monte Carlo (MC) simulations [11-18] or analytical modeling [19-25]. Owing to radiation risk, optimization of a large number of CT imaging parameters is impossible in the clinical setting. Therefore, the use of CT simulators became popular to reach the mentioned objectives. Though analytical simulations are much faster and simpler, they are not capable to accurately model physical processes, especially Compton scattering. Therefore, the application of such simulators is limited as more realistic simulations are required. Although considering all physical processes can be achieved by sophisticated MC techniques, they tend to be time-consuming. However, this problem has been nearly solved using high-performance computing and variance reduction techniques.

Although a number of studies have reported on analytical and MC simulation of CT scanners [11-25], the development of a fan-beam source model enabling to overcome the photon starvation after the collimator is still missing. Compton scattering is one of the main factors degrading image quality [26]. The accurate estimation of scattered photons magnitude and distribution and contrast detectability is impossible without a sufficient amount of photon histories [11, 18]. In this study, a fan-beam source model (FBSM) for the simulation of multi-slice fan-beam CT scanners, which has been missing in all versions of the MCNP Monte Carlo code [27] has been developed and implemented in this code. The accuracy of our new CT simulator has been verified through comparison with our previously published results.

II. Materials and Methods

A. CT Scanner Specification

The simulated CT in this work is the volumetric 64-slice GE LightSpeedTM VCT scanner (GE Healthcare Technologies, Waukesha, WI). The detailed specification of this system is presented in Table 1. The scintillator detector array consists of 58,368 individual elements configured in 64 rows of 0.0625 cm thickness on the z-axis and 0.055cm on the x-axis at isocenter. The numbers of active channel and

978-1-5386-8428-3/19/$31.00 ©2019 IEEE

reference elements are given in Table 1. The scanner uses the Performix Pro Anode Grounded Metal-Ceramic Tube Unit with two focal spots. The small and large focal spot sizes are 0.09 cm (width) × 0.07 cm (length) and 0.12 cm (width) × 0.12 cm (length), respectively. The remaining specification of the x-ray tube and system dimensions including the distances of the source to isocenter and source to the detector are presented in the following table. The acquisition parameters used to scan the phantom (described in section 2C) are shown in Table I. The reconstruction of axial slices was performed using the filtered back projection (FBP) algorithm.

TABLE I. CT SCANNER SPECIFICATION.

Source-to-image detector distance	95 cm
Source-to-isocenter distance	54 cm
Maximum fan angle	56 degrees
Maximum cone angle	4 degrees
Anode angle	7 degrees
Maximum slice thickness	2 cm at isocenter
Anode-inherent and additional filter	W-Al (3.25 mm) and Cu (0.1mm)
Tube voltage (kVp)	120
Detector material type and density	$Y_{1.34}Gd_{0.60}Eu_{0.06}O_3$, 5.95 g.cm^{-3}
Number of detector elements	58,368 (912 × 64)
Physical detector dimensions	0.97 mm × 1.1 mm × 3 mm
Detector dimenions at isocenter	0.625 mm × 0.55 mm × 3 mm
Number of active patient detectors	888 for each row
Number of reference detectors	24 for each row
Detector model	Energy integrating

B. Description of Fan-Beam Source Model and Developed MCNP-FBSM Monte-Carlo based CT simulator

MCNP is a general-purpose Monte Carlo N-Particle radiation transport code. It is one of the most widespread MC software packages for simulation of nuclear processes a pretty large community of users. Some of the specific areas of MCNP applications include radiation protection and dosimetry, radiation shielding, medical physics and detector design [27]. In this work, the MCNPX MC code was adopted to simulate the configuration of a clinical CT scanner as depicted in Table 1.

In the following, we attempt to address an important inherent limitation of MCNP/MCNP MC code in fan-beam source modeling and then devise an efficient fan-beam source model (FBSM). Thereafter, the developed MCNP-FBSM Monte Carlo-based CT simulator has been described.

Diagnostic x-ray CT imaging procedures commonly use the fan-beam geometry. The position of the focal spot of the x-ray tube, length and width of the collimator should be determined to define a specific beam shape. There are at least three methods to define the specific shape of the fan-beam in the MCNP/MCNPX Monte Carlo code. The first way is to simulate a fan-shaped beam to utilize a bunch of pencil beams including many discrete point sources [29]. The second way consists in using the cookie-cutter technique implemented in the MCNP/MCNPX code [27] which can be modeled using a spherical surface source and a cuboid cookie-cutter cell [30]. The above-mentioned methods do not consider the actual model of the focal spot. Although these approximations are acceptable for radiation dosimetry purposes, they are rather rough and crude for image quality considerations.

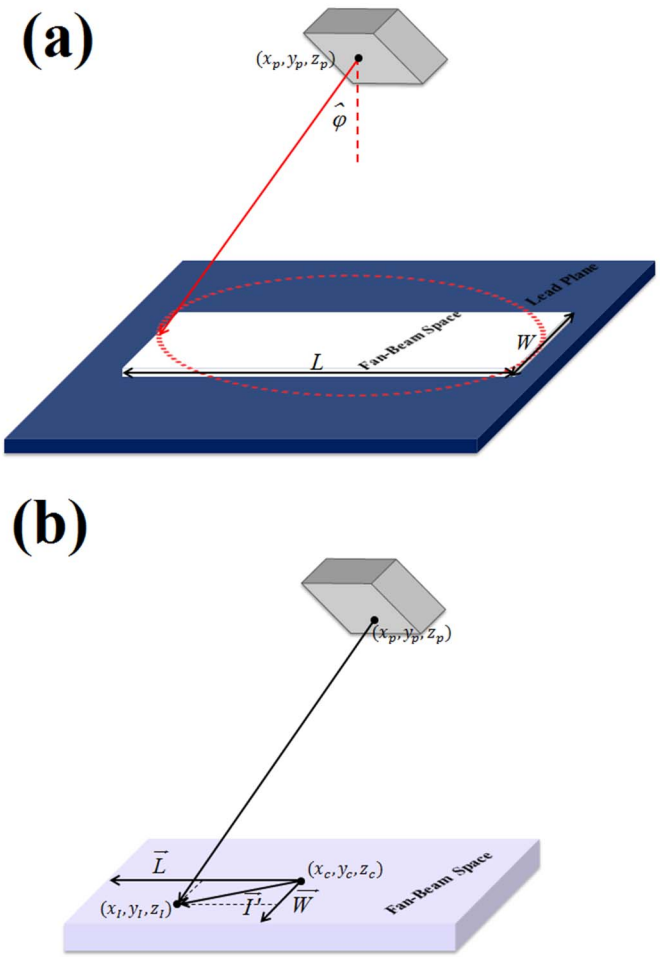

Fig. 1. A 3D representation of the MCNP standard modeling of X-ray source (a) and our purposed source model (b) for simulation of fan-beam CT scanners.

The third method, as shown in Fig. 1 (a), consists of using the collimator to change the cone-beam to fan-beam [18]. The definition of the focal spot area is possible by this method. However, depending on the size of the aperture, a large number of photons may be mostly eliminated after passing the collimator as shown in Fig. 1(a). For example, the remaining rates of photons passing through the minimum and maximum aperture size of the collimator are about 0.03 and 0.95. In this way, our devised model, as shown in Fig. 1(b), is presented to solve the above-mentioned problems. This model was directly defined for the subroutines of MCNP code. To recall this capability, the CTSRC card has been added to the dictionary of the MCNP code. An important point to note is that all default options of the standard SDEF card are enclosed in the CTSRC card as well. One can define a fan-beam source by this card as follows:

CTSRC FC=$x_c y_c z_c$; FN= $x_n y_n z_n$; FW=$x_w y_w z_w$; FL=$x_l y_l z_l$. (1)

the FC, FN, FW, and FL, as shown in Fig. 1(b), are the center of the frame, the normal vector to the frame, the frame width

and the frame length, respectively.

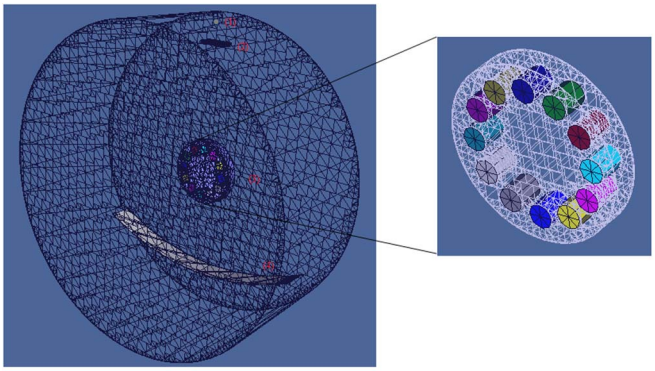

Fig. 2. A 3D representation of the MCNP-FBSM. Our model consists of the fan beam source model (1), additional and inherent filters (2), Phantom (3) and detector array (4). The location of the scoring plane was placed before the phantom.

The fan-beam angle is 56°. We have used the phase space file (PSF) technique to speed-up the MC simulation process. A scoring plane was located before the phantom (described in section 2C) to create the phase space file (PSF). First, different parameters of incoming particles (energy, weight, direction, and position) after crossing at the plane were recorded in a PSF. Second, the stored information invoked in the subsequent MCNP-FBSM executions and the photons are allowed to move the second region consisting of the phantom and detectors. Fig. 2 depicts a 3D representation of the MCNP-FBSM based CT simulator. To quantify primary and scattered photons, we have developed the perfect energy integrating detector model of Khodajou-Chokami and Sohrabpour [26] by convoluting the calculated detector efficiency.

A MATLAB program was written to generate the CT scanner geometry at various views as input files of the MCNPX MC code. Another one was written to extract signals, perform post-processing and image reconstruction. A workflow of the MCNP-FBSM based CT simulator is shown in Fig. 3.

C. Phantoms

Two types of cylindrical phantoms were utilized in this work: a Perspex water-filled cylindrical phantom having an internal diameter of 206 mm with a 6 mm wall thickness was used to compare the results of our developed MCNP-FBSM based CT simulator and experimental measurements [28] and a 250 mm diameter solid water phantom containing multi nanoparticulate contrast agents. The latter phantom containing 12 cylindrical holes was filled with different materials. To assess the detectability of contrast agents (CAS) on the resulting images, four possible CAS with high atomic numbers, namely Europium (Eu), ytterbium (Yb), osmium (Os), thallium (Tl) were considered. These materials were simulated at two levels of concentrations. K_2HPO_4 solutions with three levels of concentrations were used to simulate different types of bone tissues.

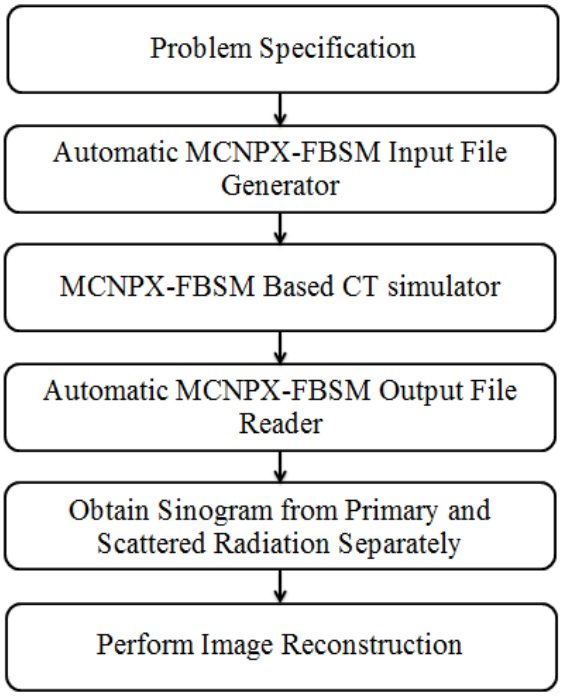

Fig. 3. Workflow of the MCNP-FBSM based CT simulator.

The fat tissue was inserted at 4 o'clock position as shown in Fig. 2. Bone materials were inserted in the phantom at 1, 2 and 3 o'clock positions with densities of 1.177, 1.413 and 1.596 g/cm^3. Likewise, Eu, Yb, Os, and Tl were inserted at 5, 6, 7 and 8 o'clock positions with low densities and at 9, 10, 11 and 12 o'clock positions with high densities, respectively. These two levels of densities of nanoparticulates CAS are summarized in Table 2.

TABLE II. SUMMARY OF LEVELS OF DENSITIES OF SIMULATED NANOPARTICULATE CAS.

Nanoparticulate CAS	**High densities (mg/cm^3)**	**Low densities (mg/cm^3)**
Europium	25.2	12.6
Ytterbium	18.8	9.4
Osmium	15.4	7.7
Thallium	12.8	6.4

III. RESULTS AND DISCUSSIONS

Fig. 4 shows the calculated unfiltered spectrum of an x-ray tube with a Tungsten anode at the 120 kV constant voltage generated using the SRS-78 program [31].

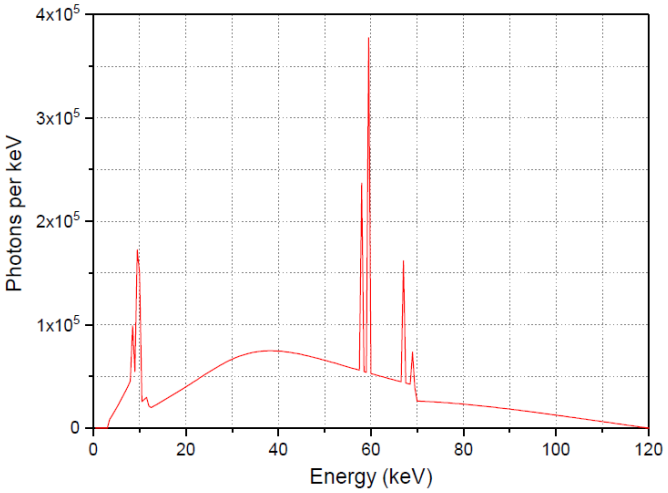

Fig. 4. Calculated unfiltered an x-ray spectrum at 120 kV constant potential.

Fig. 5 shows the calculated efficiency of the $Y_{1.34}Gd_{0.60}Eu_{0.06}O_3$ detector as a function of photon energy using our developed MCNP-FBSM Monte Carlo code.

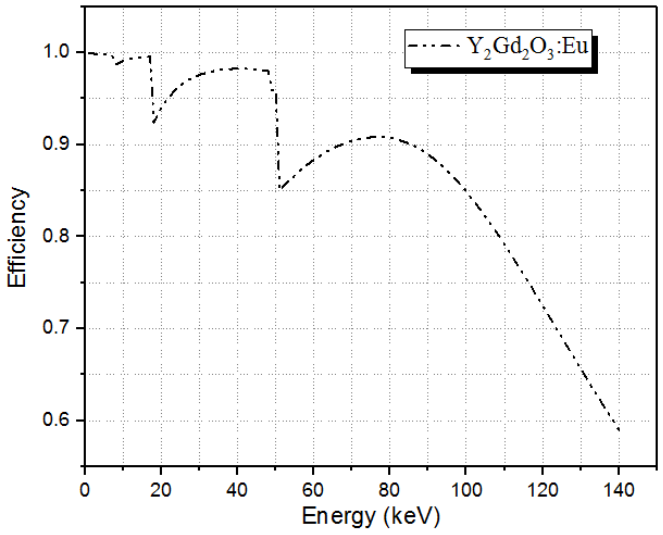

Fig. 5. Efficiency of the $Y_{1.34}Gd_{0.60}Eu_{0.06}O_3$ detector as a function of photon energy calculated by our MCNP-FBSM Monte Carlo code.

To validate our developed MCNP-FBSM based CT simulator, comparisons of the experimental and simulated scatter-to-primary ratio (SPR) have been made. The results shown in Fig. 6 demonstrate very good agreement between experimental and simulated results. Note that the experimental result was measured using the blocker array method [28].

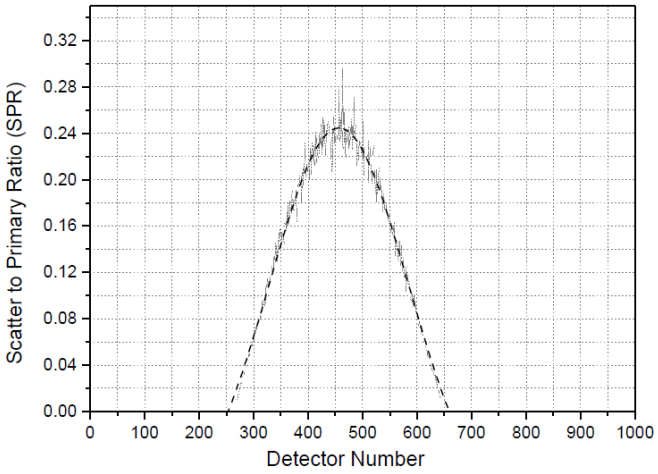

Fig. 6. Plots of the SPR as a function of detector number for the Perspex water-filled cylindrical phantom. The dashF lines indicate the measured data while the dotted lines show our simulated data.

Fig. 7 exhibits the variations of the scatter profile calculated from the 32nd detector row (the central row) using MCNP-FBSM based CT simulator. In this figure, the scatter profile is reduced to the central section of the phantom and is increased in the peripheral regions of the phantom. Presumably, this reduction results from either absorption or attenuation of most scattered photons by the phantom and thus a lower intensity arrives at the detector surface. The two peaks represent the trade-off between increasing the Compton scattering probability while increasing the transmission probability of scattered photons with decreasing the attenuation length.

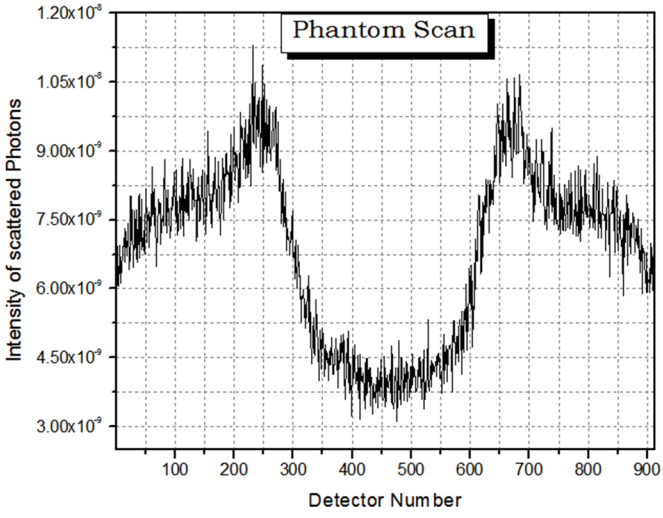

Fig. 7. Plots of the distribution of scattered photons for the multi-hole phantom as a function of detector number.

Fig. 8 shows a clear fluctuation in the SPR profile owing to the presence of different electron densities. The contrast detectability of MCNP-FBSM based simulator was investigated. Fig. 9 shows the reconstructed image of a water-filled cylindrical phantom consisting of different nanoparticulate contrast agents, various types of bones and fat. As shown in Fig. 9, low and high contrast objects are appropriately depicted, thus demonstrating the performance of our developed x-ray CT simulator.

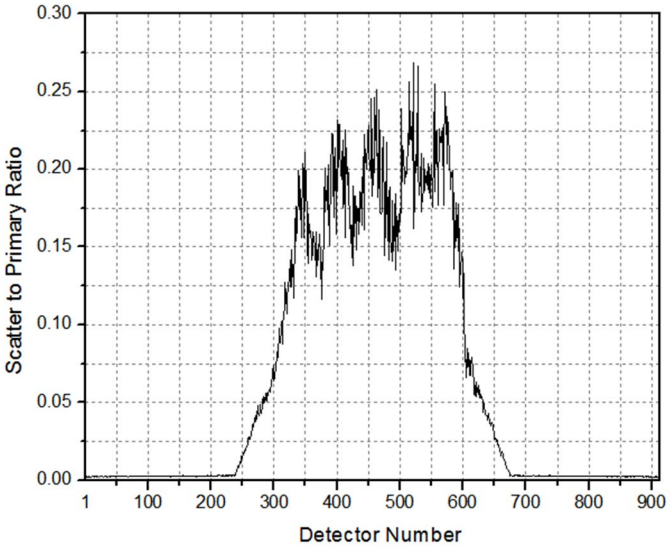

Fig. 8. Plot of the distribution of the SPR for the multi-hole phantom as a function of detector number.

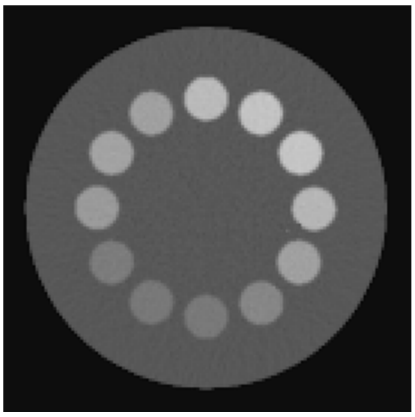

Fig. 9. Representative slice of the reconstructed images of the multi-hole phantom from simulated projections containing several contrast agents.

IV. Conclusions

We have developed a novel computationally efficient fan-beam source model (FBSM) for the simulation of multi-slice fan-beam CT scanners. There is no need to use the collimator in the system configuration when using the FBSM model, which enables to overcome the perennial problem of particle starvation induced by the collimator. In addition, a new MCNP-FBSM based CT simulator has been developed by adding the FBSM capability to the subroutines of the standard MCNP MC code. The accuracy of our model has been evaluated through comparison with the experimental result, demonstrating good agreement. Our MCNP-FBSM based CT simulator is a versatile tool for scanning protocol evaluation, optimization of geometrical design parameters, assessment of image reconstruction algorithms and evaluation of the impact of future innovations [32] attempting to improve the performance of CT scanners.

References

[1] S. C. Lee, H. K. K. Kim, I. K. Chun, M. H. Cho, S. Y. Lee and M. H. Cho "A flat-panel detector based micro-CT system: performance evaluation for small-animal imaging," Phys. Med. Biol. vol 48, pp. 4173–85, 2003.

[2] M. Drangova and A. Fenster "A laboratory CT scanner for dynamic imaging," Med. Phys. vol. 21, pp. 731–40, 1994.

[3] Y. Kyriakou, E. Meyer, D Prell and M Kachelriess "Empirical beam hardening correction (EBHC) for CT," Med. Phys. vol. 37 pp. 5179–87, 2010.

[4] J. D. Evans, B. R. Whiting, D. G. Politte, J. A. O'Sullivan, P. F. Klahr and J. F. Williamson "Experimental implementation of a polyenergetic statistical reconstruction algorithm for a commercial fan-beam CT scanner," Phys. Med. vol. 29 pp. 500-12, 2013.

[5] J. P. Schlomka et al "Experimental feasibility of multi-energy photon-counting K-edge imaging in pre-clinical computed tomography," Phys. Med. Biol. vol. 53 pp. 4031–47, 2008.

[6] P. M. Shikhaliev "Energy-resolved computed tomography: first experimental results," Phys. Med. Biol. vol. 53 pp. 5595–613, 2008.

[7] P. M. Shikhaliev "Photon counting spectral CT: improved material decomposition with K-edge-filtered x-rays," Phys. Med. Biol. vol. 57 pp. 1595–615, 2012

[8] P. H. Jeon, C. L. Lee, D. H. Kim, Y. J. Lee, S. S. Jeon and H. J. Kim "Dose reduction and image quality optimizations in CT of pediatric and adult patients: phantom studies," J. Instrum. vol.9 P03013, 2014.

[9] P. Ning, P. Zhu, D. Shi, Y. Guo and M. Sun "X-Ray Dose Reduction in Abdominal Computed Tomography Using Advanced Iterative Reconstruction Algorithms," PloS One vol.9 pp. E92568, 2014.

[10] Z. Yu, S. Leng, S. M. Jorgensen, Z. Li, R. Gutjahr, B. Chen, X. Duan, A. F. Halaweish, L. Yu, E. L. Ritman, C. H. McCollough "Initial results from a prototype whole-body photon-counting computed tomography system," Proc SPIE Int Soc Opt Eng. 9412, 2015.

[11] D. V. Eeden and F. D. Plessis "EGS_cbct: Simulation of a fan beam CT and RMI phantom for measured HU verification," Phys. Med. vol. 32 1375-80, 2016.

[12] M. Müllner, H. Schlattl, C. Hoeschen, O. Dietrich "Feasibility of spectral CT imaging for the detection of liver lesions with gold-based contrast agents – a simulation study," Phys. Med. vol. 31 pp. 875-81, 2015.

[13] M. Khodaverdi, A. F. Chatziioannou, S. Weber, K. Ziemons, H. Halling and U. Pietrzyk "Investigation of different microCT scanner configurations by GEANT4 simulations," IEEE Trans. Nucl. Sci. vol. 52 pp. 188–92, 2005.

[14] A. P. Colijn, W. Zbijewski, A. Sasov and F. J. Beekman "Experimental validation of a rapid Monte Carlo based micro-CT simulator," Phys. Med. Biol. vol. 49 4321–33, 2004.

[15] K. H. Chang, W. Lee, D. M. Choo, C. S. Lee and Y. Kim "Dose reduction in CT using bismuth shielding: measurements and Monte Carlo simulations," Radiat Prot Dosimetry vol. 138 382–388, 2010.

[16] R. A. Nasirudin, K. Mei, P. Penchev, A. Fehringer, F. Pfeiffer, E.J. Rummeny, M. Fiebich, P. B. Noël "Reduction of metal artifact in single photon-counting computed tomography by spectral-driven iterative reconstruction technique," PloS One. vol. 10 E0124831, 2015a.

[17] R. A. Nasirudin, P. Penchev, K. Mei, E. J. Rummeny, M. Fiebich, P. B. Noel "A Monte Carlo software bench for simulation of spectral k-edge CT imaging: Initial results," Phys Med vol. 31 398– 405, 2015b.

[18] M. R. Ay and H. Zaidi, Development and validation ofMCNP4C-based Monte Carlo simulator for fan- and cone-beam x-ray CT, Phys. Med. Biol. **50**, 4863–4885, 2005.

[19] W. P. Segars, B. M. Tsui, E. C. Frey, G. A. Johnson, S. S. Berr "Development of a 4-D digital mouse phantom for molecular imaging research," Mol Imaging Biol. vol. 6 pp. 149-59 2004.

[20] W. P. Segars, M. Mahesh, T. J. Beck, E. C. Frey, B. M. Tsui "Realistic CT simulation using the 4D XCAT phantom," Med Phys vol. 35 pp. 3800-8, 2008.

[21] D. De Francesco and A. Da Silva "Multislice spiral CT simulator for dynamic cardiopulmonary studies," SPIE Medical Imaging 2002: Physiology and Function from Multidimensional Images (San Diego, CA, USA) SPIE vol.4683 pp.305-16, 2002.

[22] J. Hsieh "Analytical models for multi-slice helical CT performance parameters," Med. Phys. vol. 30 pp. 169-78, 2003.

[23] P. M. Shikhaliev "Beam hardening artefacts in computed tomography with photon counting, charge integrating and energy weighting detectors: a simulation study," Phys. Med. Biol. vol. 50 pp. 5813–27, 2005.

[24] J. Zhu, S. Zhao, Y. Ye and G. Wang 2005 "Computed tomography simulation with superquadrics," Med. Phys. vol. 32 pp. 3136-43.

[25] R. L. Dixon, M. T. Munley and E. Bayram "An improved analytical model for CT dose simulation with a new look at the theory of CT dose," Med. Phys. vol. 32 p.3712, 2005.

[26] H. Khodajou-Chokami, M. Sohrabpour "Design of linear anti-scatter grid geometry with optimum performance for screen-film and digital mammography systems," Phys. Med. Biol. vol.60 p.5753, 2015.

[27] D. B. Pelowitz, "MCNPX User's Manual version 2.7.0," Los Alamos Laboratory Report, 2011.

[28] A. Akbarzadeh et al, Measurement of scattered radiation in a volumetric 64-slice CT scanner using three experimental techniques, Phys. Med. Biol. **55** 2269–2280, 2010.

[29] A Khursheed, M C Hillier, P C Shrimpton and B F Wall, Influence of patient age on normalized effective doses calculated for CT examinations, Br. J. Radiol. 75 819–30, 2002.

[30] J Gu, B Bednarz, P F Caracappa and X G Xu "The development, validation and application of a multi-detector CT (MDCT) scanner model for assessing organ doses to the pregnant patient and the fetus using Monte Carlo simulations," Phys. Med. Biol. 54 2699–2717, 2009.

[31] K. Cranley, B. J. Gilmore, G. W. A. Fogarty and L. Desponds "IPEM Report 78: Catalogue of Diagnostic X-ray Spectra and Other Data," (CD-Rom Edition 1997) (Electronic Version prepared by D Sutton) (York: The Institute of Physics and Engineering in Medicine (IPEM)), 1997.

[32] H. Khodajou-Chokami, S. A. Hosseini, M. R. Ay, A Safarzadehamiri, P. Ghafarian, and H. Zaidi, "A Novel Method for Measuring the MTF of CT Scanners: A Phantom Study," the 14th IEEE International Symposium on Medical Measurements and Applications, 2019.